J Mater Sci (2007) 42:1190–1195
DOI 10.1007/s10853-006-1436-2

Manganese pigmented anodized copper as solar selective absorber

L. Arurault · M. H. Belghith · R. S. Bes

Received: 5 September 2004 / Accepted: 13 April 2006 / Published online: 18 January 2007

Abstract The study concerns the optical and structural properties of layers obtained by a new efficient surface treatment totally free of chromium species. The process is made up of an anodic oxidation of copper in an alkaline solution followed by an alkaline potassium permanganate dipping post-treatment. Coatings, obtained at the lab and pilot scales, are stable up to 220 °C in air and vacuum, present low emissivity (0.14 at 70 °C) and high solar absorptivity (0.96), i.e. a suitable thermal efficiency (0.84 at 70 °C).

Introduction

Many attempts have been made in our research team to develop treatment processes of various substrates (stainless steels, zinc, aluminium alloys) in order to obtain solar selective surfaces [1–3]. But copper appears like one of the most interesting substrates due to its good capability towards shaping.

Selective copper-black layers have been obtained so far by painting, by chemical conversion, by electrochemical conversion or by thermal oxidation [4–8]. But the traditional copper-black surface is reported to be stable only below 200 °C with an absorptivity $\alpha = 0.94$ and an emissivity $\varepsilon = 0.14$, i.e. a thermal efficiency $\eta = 0.82$ at 70 °C [9].

This paper describes the optical and structural properties as well as thermal stability tests of layers prepared at the lab and pilot scales by a new surface treatment process, totally free of chromium species, based upon an electrochemical oxidation followed by an appropriate chemical post-treatment [10].

L. Arurault (✉) · R. S. Bes
Centre Interuniversitaire de Recherche et d'Ingéniérie des Matériaux (CIRIMAT), UMR 5085, CNRS/INPT/UPS, Laboratoire de Chimie des Matériaux Inorganiques et Energétiques (LCMIE), Université Paul Sabatier, 118 Route de Narbonne, 31062 Toulouse Cedex 09, France
e-mail: arurault@chimie.ups-tlse.fr

M. H. Belghith
Jacques Giordano Industries, Z.I. Les Paluds, Aubagne 13400, France

Experimental procedures

Surface preparation

Phosphorus (0.2 wt.%) deoxidized copper is used as substrate. A single foil ($40 \times 50 \times 0.15$ mm) is used each run at the lab scale while three sheets ($87 \times 300 \times 0.15$ mm each one) operated simultaneously at the pilot scale.

Samples are initially degreased by dipping in $C_2H_3Cl_3$ solution during 5 min. and rinsing with deionized water at room temperature. An aqueous nitric acid solution (20 wt.%) at 60 °C is used for chemical etching during 1.5 min., followed by rinsing with deionized water.

This pre-treatment step is followed by the main treatment, an anodizing during 15 min. at 60 °C in an aqueous electrolyte made of NaOH (10 wt.%) and $NaClO_2$ (5 wt.%) in order to produce a strong, fast and reproducible oxidation of the copper substrate simultaneously by chlorite chemical reaction and by electrochemical anodic polarization. The electrochemical

cell is made up of the copper sample as the anode, the Hg/HgO electrode as reference, while platinum or graphite are used as cathode, respectively, at lab scale and pilot scale. The anodizing potential was +0.75V/ref., while nitrogen was used as bubbling gas in the pilot experiments in order to avoid contamination of the bath by atmospheric CO_2 and to obtain a better electrolyte homogeneity.

After rinsing with deionized water, the samples are immersed in an aqueous solution made up of NaOH (3 wt.%) and $KMnO_4$ (3 wt.%) at 50 °C for 4 min, and finally dried at 90 °C for 15 min. before any characterization. The aim of this post-treatment step is to stabilize the coating, using an additional oxidation electrolyte without chromium, contrary to previous work [11].

Characterization

Optical properties, total solar absorptivity α and total hemispherical emissivity ε_{70} (at 70 °C), are measured using an absorptiometer and an emissiometer (EL510, EL520, Elan Informatique) as well as they are calculated from reflectance curves in the wavelength range 0.25–21 μm (VARIAN CARY 2300 and NICOLET FTIR 800 spectrophotometers) by standard methods using AM1 solar spectral irradiance. The two methods give the same results within experimental errors. So the thermal efficiency η of the surface at 70 °C is then deduced using the following relation [8]:

$$\eta = \alpha - 0.85\varepsilon_{70} \quad (1)$$

A value for $\eta \geq 0.80$ is characteristic of a solar selective surface [8].

Structural characterization is carried out by scanning electron microscopy coupling with Xray energy dispersive spectroscopy (SEM/X-EDS, JEOL J.M. 6400 device) and by secondary ion mass spectroscopy (SIMS, Cameca MS46). Additional analytical informations are obtained from glancing RX diagrams ($0.2° \leq \alpha \leq 2°$, D500 Siemens diffractometer) and from Fourier transform infrared (FTIR) spectra in the range 4000–200 cm^{-1} (NICOLET FTIR 710 spectrophotometer).

Thermal stability tests are conducted in atmosphere (open system) and under vacuum (10^{-3} Torr) at different temperatures up to 230 °C and time durations up to 10 days. In use, the optical properties of selective surfaces must remain absolutely constant. Thus flat collectors must be able to withstand short exposures to their stagnation temperature, i.e. about 150 °C for collectors working in air and up to 220 °C for collectors working under vacuum.

Textural analysis of the coating is carried out by electrochemical impedance spectroscopy (EIS), plotting NYQUIST diagram in 65 kHz–1 MHz frequency range. The electrolyte is a Na_2SO_4 aqueous solution (0.1 M) at 20 °C, while platinum plate is used as counter-electrode and $Hg/Hg_2SO_4,K_2SO_4$ electrode as reference. The potential at the working electrode (1 cm^2) is –1.2 V/ref, using SCHLUMBERGER 1286 and 1250 types potentiostat and frequency analyzer.

Results and discussion

Optical properties

Effectiveness of the post-treatment

Figure 1 shows the reflectance spectrum for samples before and after the post-treatment step. In the visible wavelength range, there is an important reduction of the reflectance for the post-treated sample while minus change can be seen in the IR wavelength range. These results correspond in fact to an improvement of the α value while the ε value is unaffected. For the post-treated sample, $\alpha = 0.96$ and $\varepsilon_{70} = 0.14$ giving a thermal efficiency $\eta_{70} = 0.84$, i.e. a value characteristic of a solar selective surface. So the post-treatment is efficient, inducing probably a stabilization of the coating chemistry through the CuO formation that usually increases the solar absorption by its low reflectance in the visible wavelength [11].

Thermal stability

Figure 2 shows optical properties of the surface submitted to heat treatment in air during 5 and 10 days at

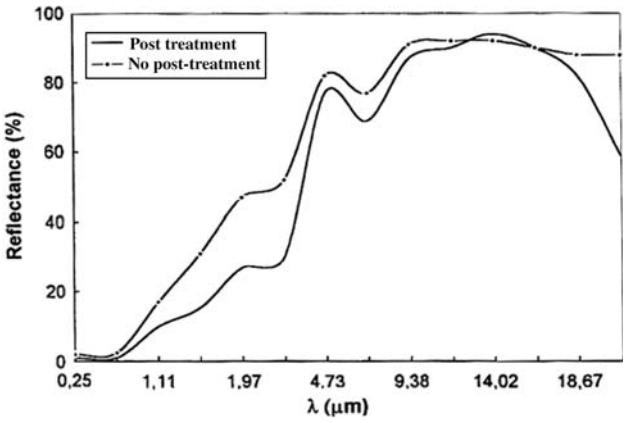

Fig. 1 Reflectance spectrum for samples before and after the post-treatment step

various temperatures. Increase of temperature (25–230 °C) results in a slow decrease of both α and ε_{70} up to about 200 °C, i.e. a temperature more greater than the stagnation temperature of flat solar collectors working in air. Above 200 °C, the decrease of optical properties is more pronounced but the surface is always a selective one at 220 °C ($\alpha = 0.87$, $\varepsilon_{70} = 0.08$ and $\eta_{70} = 0.80$).

The optical properties are also measured in vacuum during 10 days (Fig. 3) at 220 °C, i.e. close to the stagnation temperature of flat solar collectors working under vacuum. If α decreases slowly, it appears at about 5 days that ε_{70} reach a minimum. So from about 7 days the selective property of the surface is destroyed ($\eta_{70} < 0.80$).

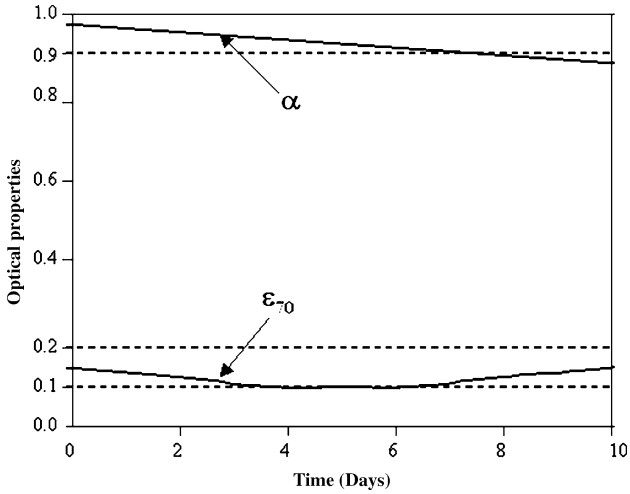

Fig. 3 Optical properties after heat treatment under vacuum (10^{-3} Torr) at 220 °C as a function of time duration

Chemical composition

SIMS profiles

Distribution of the metallic elements as a function of the abrasion time, so of the depth in the conversion layer, reveals a concentration gradient of metals. The profiles obtained bring to light several zones:

- a surface zone which corresponds to a very short abrasion time for which the ionic intensity of all the species is extremely high;
- a deep zone constituted by two parts, named outer and inner (Fig. 4); for this last one the ionic intensity of the species decreases close to the substrate.

Previous analytical studies [12–15] show that the anodic coating have a varied and complex composition including Cu_2O, CuO, $Cu(OH)_2$ and others metastable compounds notably depending of the complexing power of the electrolyte. In comparison to the profiles obtained with the coating elaborated without post-treatment (Fig. 4), the profiles relative to the selective coating (Fig. 5) reveal the presence of Mn and K as well as important modifications of the relative composition of main species. Moreover for a coating heated at 220 °C in air during 10 days, the profiles (Fig. 6) indicate also significant modifications of relative composition mainly from the Cu signal which present a sharp maximum in the deep zone.

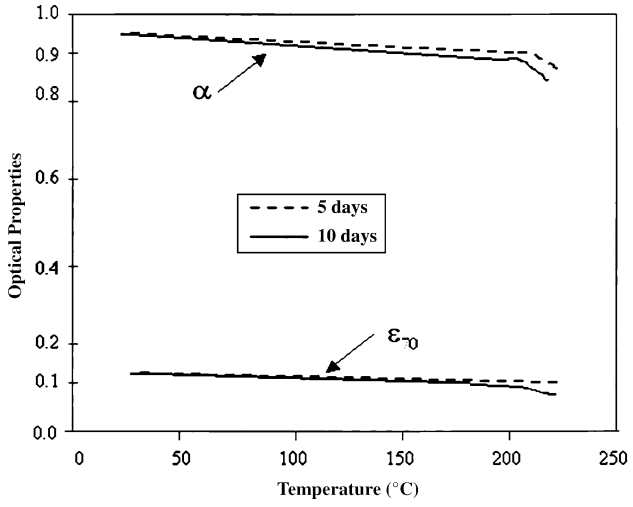

Fig. 2 Optical properties after heat treatment in air (5 and 10 days) as a function of temperature

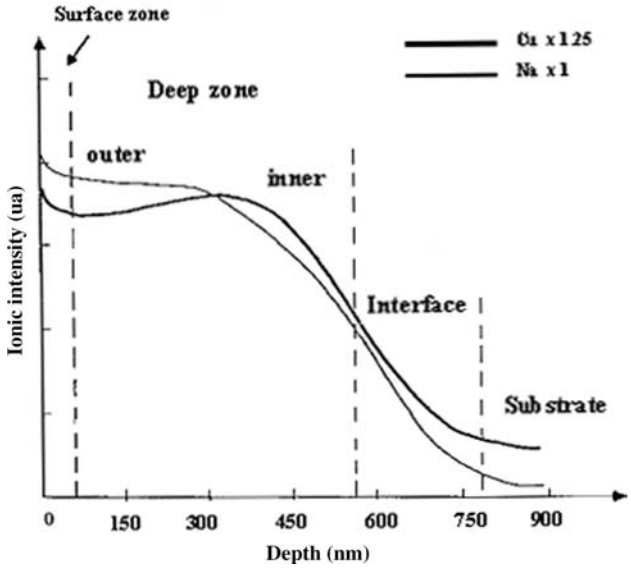

Fig. 4 SIMS profiles of metals before the post-treatment step

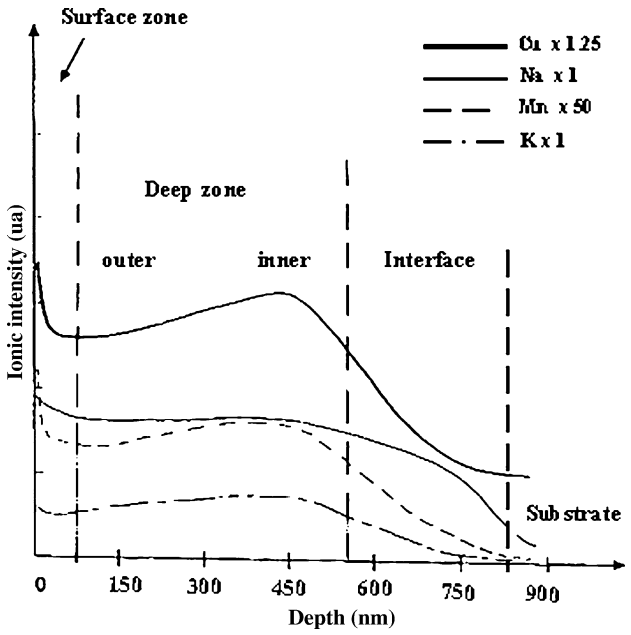

Fig. 5 SIMS profiles of metals after the post-treatment step

Additional analytical results

Additional results have been obtained from glancing RX diagrams, FTIR spectra and SEM/X-EDS spectra. They confirm that the copper-black coating is mainly made of CuO oxide [16] and traces of copper II salts (chlorides and nitrates). After heat treatment in vacuum at 200 °C the spectra are unaffected, while for heat treatment in air at 220 °C, these three analytical techniques indicate the presence of an additional copper I oxide, resulting probably from the transitory formation of Cu_3O_2 [17, 18], i.e. a metastable compound [19], the decomposition of which conducts to CuO and Cu_2O [20].

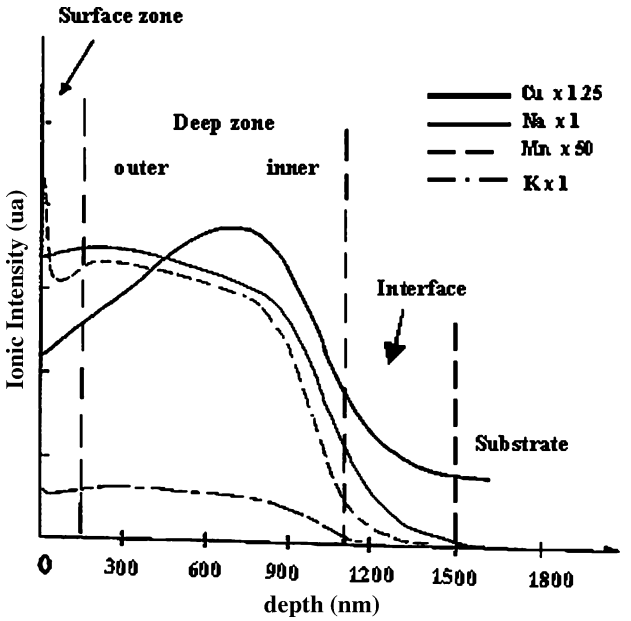

Fig. 6 SIMS profiles of metals after heat treatment in air at 220 °C during 10 days

Microstructure and porosity

SEM study

SEM micrograph (Fig. 7) shows a typical conversion coating. The predominant morphology consists of a small-scale roughness, including needle-like grains and voids apparently present throughout the thickness of the selective coating. The grains are usually 1.0 μm in length while the average diameter is 0.1 μm. Although the thickness of the selective coating increase by the heat treatments, its microstructure is apparently not really affected. So the previous variation of optical properties result probably from the above change in the chemical composition of the coating with heat treatment.

EIS study

The porosity is then particularly studied using EIS analysis. NYQUIST diagram in the high frequency (HF) range (Fig. 8) reveals the presence of local diffusion phenomena characteristics of the coating porosity, the observed arc accounting for spherical or occluded pores [21]. At medium frequency (MF), the capacitive loop is characteristic of a charge transfer process at the electrode-solution interface [22]. These results allow then to propose an equivalent electric scheme of the electrolyte-coating-substrate interfaces

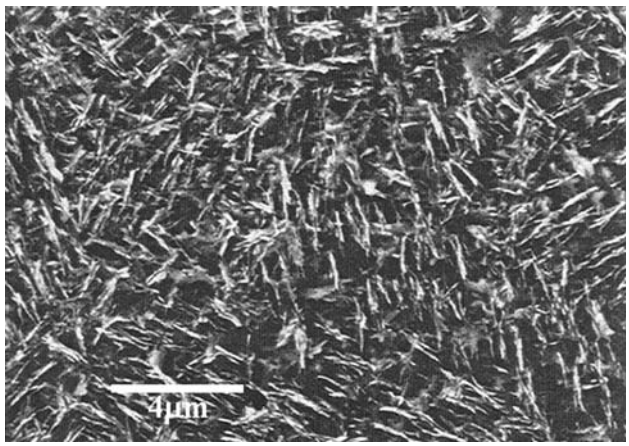

Fig. 7 SEM micrograph of a typical conversion coating

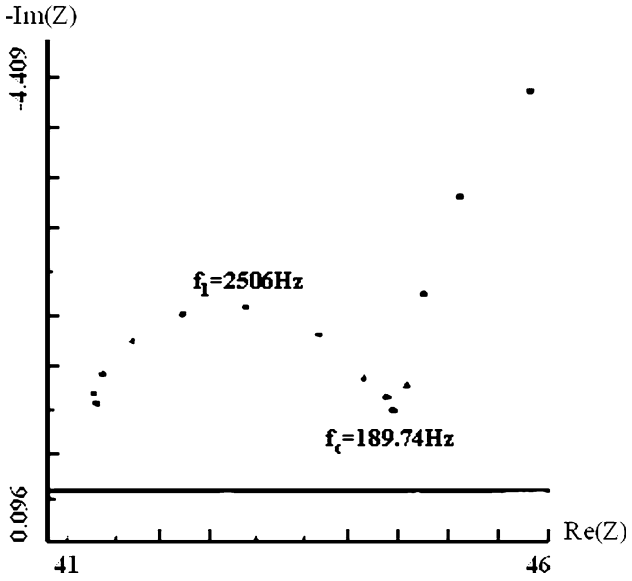

Fig. 8 High frequency part of the Nyquist diagram and beginning of the capacitive loop in the medium frequency range

(Fig. 9) where R_e is the electrolyte resistance, R_d and C_d account for the diffusion of the electrolyte in the pores and R_t and C_t represent the charge transfer process. The best values of the electric components as well as the characteristic angular frequencies ω_0, ω_1 and ω_c are then obtained by fitting the experimental impedance curves. Assuming identical pores, the characteristic dimensions of the coating are related to the electrolyte and the impedance spectra by the two relations [23]:

$$\frac{L^2}{r} = \frac{R_t}{2\rho_e}\frac{\omega_0}{\omega_c} \tag{2}$$

and

$$\frac{L}{r^2} = \frac{3\pi P R_d}{\rho_e} \tag{3}$$

where L is the pore depth, assumed to be the coating thickness, r is the aperture radius of the pore, ρ_e is the electrolyte resistivity and P is the pore density. L being first estimated from SIMS profiles, r and P are then calculated before and after heat treatment (Table 1). The results show that the aperture radius of the pores and the density of pores stay constant in spite of the air heat treatment, while the pores diameter seems to increase under vacuum conditions probably due to better dehydration. Furthermore, it appears through these calculations that the nanoporosity should have no influence on the optical properties because the pore diameter is lower than the solar wavelength.

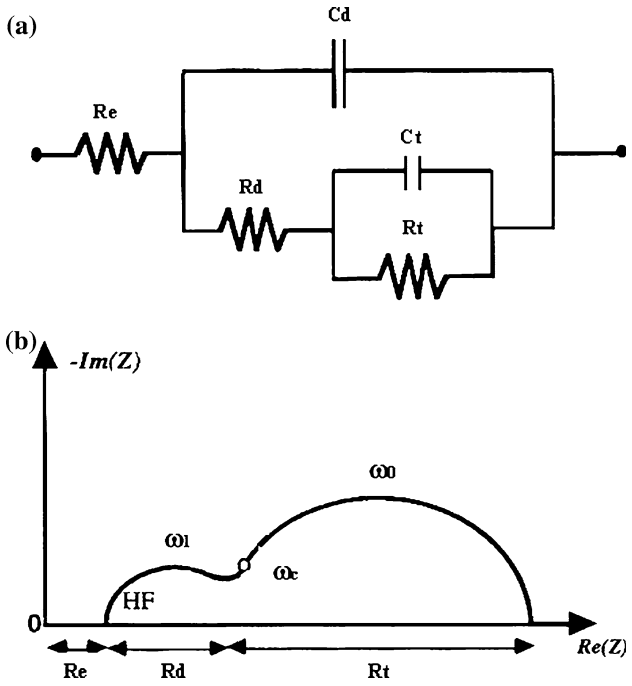

Fig. 9 Equivalent electric scheme (**a**) and corresponding theoretical Nyquist diagram (**b**)

Comparison of the lab and pilot scales

At the pilot scale, optical properties on different points of the three sheets are measured in order to appreciate the homogeneity of the treatment. Figure 10 shows typical results obtained on one sheet: within experimental errors, α and ε_{70} values are similar (0.95 and 0.13, respectively) whatever the location on the sheet and whatever the sample. The selective surface is so homogeneous and the reproducibility of the process is good. Furthermore, the optical properties are the same that the previous values obtained at the lab scale ($\alpha = 0.96$ and $\varepsilon_{70} = 0.14$).

SEM and EIS characterizations give similar results; nevertheless SIMS profiles indicate only the increase of the coating's thickness at the pilot scale in comparison with the lab scale. The physico-chemical characteristics of the coating are so unchanged with the scale change,

Table 1 Estimated characteristics of the layers

Layer	L (nm)	r (nm)	P (10^{11} m^{-2})
Copper-black coating	800	11	14.3
Heat treatment: air, 220 °C, 10 days	1500	10	15.1
Heat treatment: vacuum, 220 °C, 10 days	1200	17	11.6

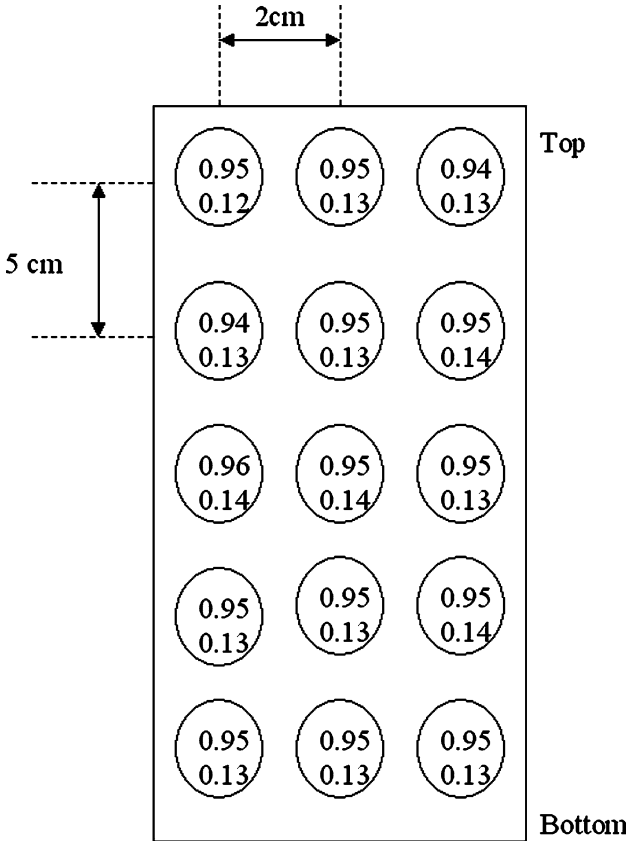

Fig. 10 Optical properties on various locations for one of the sheets treated at the pilot scale (mean values: $\alpha = 0.95$ and $\varepsilon_{70} = 0.13$)

except for the improvement of coating's thickness, probably due to the use of an electrolyte with better homogeneity and free of atmospheric gases using nitrogen gas bubbling. So these results appear very interesting in view of the process scaling up.

Conclusion

Black coating were prepared, at the lab and pilot scales, by anodization of copper in NaOH, $NaClO_2$ bath at 60 °C using nitrogen as bubbling gas, then by dipping in a NaOH, $KMnO_4$ bath at 50 °C.

Analysis revealed that these coatings are mainly made up of CuO oxide and indicated the presence of an additional metastable copper I oxide, probably Cu_3O_2, which converts finally to CuO and Cu_2O.

The coatings may be used as solar selective absorber with low emissivity (0.14 at 70 °C), high solar absorptivity (0.96) and good thermal efficiency (0.84 at 70 °C). The coatings are stable up to 220 °C in air and vacuum (10^{-3} Torr) for a sufficient long time to prevent any malfunction of the solar collector (stagnation temperature).

Acknowledgements The authors greatly appreciate financial support of ADEME and Région Midi-Pyrénées, France.

References

1. Komla A, Aries L, Naboulsi B, Traverse JP (1991) Solar Energy Mat 22:281
2. Konate S, Bes RS, Traverse JP (1997) Ann Chim Sci Mat 22:67
3. Salmi J, Bonino JP, Bes RS (2000) J Mat Sci 35:1347
4. US PATENT US4309257, January 5th, 1982
5. Scherer A, Inal OT, Pettit RB (1988) J Mat Sci 23:1923
6. Roos A, Karlsson B (1983) Solar Energy Mat 7:467
7. Roos A, Georgson M (1991) ibid 22:29
8. Richharia P, Chopra KL, Bhatnagar MC (1991) ibid 23:93
9. Pekruhn W, Thomas LK, Broser I, Schroder A, Wenning U (1985) ibid 12:199
10. FR. PATENT FR9508090, 29 August 1997; FR. PATENT D FR00/022293, February 22th, 2000
11. Hörnström SE, Karlsson SE, Roos A, Westerstrandh B, Kamf A (1984) Solar Energy Mat 9:367
12. Royer RJ, Kleinberg J, Davidson AW (1957) J Inorg Nucl Chem 4:115
13. Shams El Din AM, Abd El Wahab FM (1964) Electrochim Acta 9:113
14. Abrantes LM, Castillo LM, Norman C, Peter LM (1984) J Electroanal Chem 163:209
15. Mayer ST, Muller RH (1992) J Electrochem Soc 139(2):426
16. Lefez B, Souchet R, Kartouni K, Lenglet M (1995) Thin Solid Films 268:45
17. Machefert JM, Lenglet M, Blavette D, Menand A, D'Huysser A (1989) In: Morterra C, Zecchina A, Costa G (eds) Structure and reactivity of surfaces, Elsevier Science Pub, p 625
18. Lenglet M, Kartouni K, Machefert J, Claude JM, Steinmetz P, Beauprez E, Heinrich J, Celati N (1995) Mater Res Bull 30:393
19. Carel C, Mouallem-Bahout M, Gaudé J (1999) Solid State Ionics 17:47
20. Lenglet M, Kartouni K (1993) Revue de Métallurgie CIT/SGM, Décembre, p 1637 (in french)
21. Keiser H, Beccu KD, Gutjahr MA (1976) Electrochim Acta 21:539
22. Amstrong RD, Edmondson K, Lee JA (1975) J Electroanal Chem 63:287
23. Komla A (1991) Ph.D. Thesis, Paul Sabatier University, Toulouse, France